10-9-2009

Gravity Wave Ducting in the Upper Mesosphere and Lower Thermosphere Duct System

R. L. Walterscheid
The Aerospace Corporation

Michael P. Hickey Ph.D.
Embry-Riddle Aeronautical University, hicke0b5@erau.edu

JOURNAL OF GEOPHYSICAL RESEARCH, VOL. 114, D19109, doi:10.1029/2008JD011269, 2009

Gravity wave ducting in the upper mesosphere and lower thermosphere duct system

R. L. Walterscheid[1] and M. P. Hickey[2]

Received 8 October 2008; revised 11 June 2009; accepted 23 June 2009; published 9 October 2009.

[1] We report on a numerical study of gravity wave propagation in a pair of ducts located in a region where dramatic changes in the airglow most likely associated with ducted wave trains are observed. We examine ducting in an upper mesosphere inversion (INV) and an always present lower thermosphere stable layer (LTD) for a range of phase speeds and horizontal wavelengths characteristic of ducting events. We analyze the propagation and modal structure of ducted waves for backgrounds with increasing realism, starting with a climatological temperature profile where only the LTD is present. In succession, we add the INV based on the work of Smith et al. (2003), climatological winds, and winds in the upper mesosphere based on the work of Smith et al. (2003). We examine ducting for phase speeds between 40 and 100 m s^{-1} and horizontal wavelengths between 20 and 60 km. We find that without winds, only the LTD supports ducting of waves forced from below. When observed winds and temperatures are included, strong ducting is evident in both regions. For waves forced from below, the strongest ducted modes are those with slower phase speeds, and of these the third gravest agree reasonably well with the observed phase speeds and wavelengths, indicating that the observations are consistent with linear ducted waves. For waves forced in the INV, we find an intense and strongly dominant fundamental mode. This is a fast mode having phase speeds $\sim$100 m s^{-1} for a horizontal wavelength of 30 km in the INV and much faster in the LTD. That the fundamental is not seen in Smith et al.'s (2003) observations indicates that the waves were forced from below and that the lowest mode was blocked by an evanescent barrier below the INV. Our results show that the two ducts communicate: the upward extensions of waves ducted in the INV are seen in the LTD. This is particularly significant in the case of in situ forcing, where the fundamentals combine to give amplification exceeding a factor of 10 in the LTD.

Citation: Walterscheid, R. L., and M. P. Hickey (2009), Gravity wave ducting in the upper mesosphere and lower thermosphere duct system, *J. Geophys. Res.*, *114*, D19109, doi:10.1029/2008JD011269.

1. Introduction

[2] There have been instances of sudden brightening of the airglow layer (sometimes referred to as walls) that appear to propagate across the sky [*Taylor et al.*, 1995a; *Hecht et al.*, 1995; *Swenson et al.*, 1998; *Smith et al.*, 2003, 2005], the more dramatic of which have been attributed to mesospheric bores [*Dewan and Picard*, 1998; *Smith et al.*, 2003, 2005]. These events clearly depend on ducting since otherwise it would not be possible to maintain a strong horizontally propagating wave train over large distances. *Smith et al.*'s [2003] event in particular was tracked over a distance that was far too large for waves to first reach the airglow layers at the points where they were observed in the airglow.

[3] There is always a deep stable layer in the lower thermosphere that is typically not too far above where the upper mesospheric inversions are located [*Walterscheid et al.*, 1999; *Smith et al.*, 2003, 2005; *She et al.*, 2004]. For a bore to travel in a mesospheric inversion it must be isolated from the stable layer $\sim$10–15 km above.

[4] We analyze the modal structure of ducted waves for backgrounds with increasing realism, starting with a climatological temperature profile [*Hedin*, 1991] where the only duct is in the lower thermosphere (LTD). In succession we add an upper mesospheric inversion (INV) based on observations during a strong ducting event [*Smith et al.*, 2003], climatological winds [*Hedin et al.*, 1996], and winds in the upper mesosphere based on the observations from *Smith et al.* [2003]. We loosely refer to the regions where the Brunt-Väisälä frequency squared (N^2) profile has a distinct maximum as ducts, even if, because of winds, for example, ducting does not occur. Also, we may use the terms INV or

[1]Space Science Applications Laboratory, The Aerospace Corporation, Los Angeles, California, USA.
[2]Department of Physical Sciences, Embry-Riddle Aeronautical University, Daytona Beach, Florida, USA.

0148-0227/09/2008JD011269$09.00

LTD to identify an altitude region whether or not for a specific run an N^2 maximum occurs there.

2. Theory and Modeling

[5] Ducted gravity waves are vertically trapped internal gravity waves that can be sustained with little diminishment in the absence of forcing. Fully ducted waves (no leakage or loss of energy) are resonant waves trapped by evanescence, rapid vertical variations in the background state, or rigid surfaces. Nonresonant waves cannot exist as permanent free waves and will decay without continuous forcing. To be resonant the waves must fit in the region of wave trapping. Fitting means that the wave must be able to satisfy certain continuity conditions at the boundaries of the duct [*Francis*, 1973].

[6] Ducts where wave trapping is caused primarily by variations in N are thermal ducts, while ducts where trapping is caused primarily by wind gradients are Doppler ducts [*Francis*, 1973; *Richmond*, 1978; *Schubert and Walterscheid*, 1984; *Chimonas and Hines*, 1986; *Isler et al.*, 1997]. Winds have their maximum effect when aligned with the direction of wave propagation and have no effect when normal to the winds.

[7] We examine internal waves in layers trapped by evanescence above and below. We use two models. The first is an idealized model where the duct is represented by three layers of constant m^2: A layer of $m^2 > 0$ surrounded by two semi-infinite layers of $m^2 < 0$. For a greater degree of realism we use our full-wave model [*Walterscheid et al.*, 1999; *Hecht et al.*, 2001; *Hickey*, 2001]. This model includes dissipation and wave reflection realistically.

2.1. Three-Layer Model

[8] Here we examine ducting in an idealized model to help interpret the results of the full-wave model with its greater complexity. We assume waveform solutions of the form $\psi = \hat{\psi}(z)\overline{\rho}^{-1/2} \exp i(kx - \omega t)$, where ω is frequency, x and z are, respectively, the horizontal and vertical coordinates, $\overline{\rho}$ is basic-state density and t is time. The relation governing the vertical component of the velocity w derived from the linearized equations of motion is

$$\hat{w}'' + m^2\hat{w} = 0, \tag{1}$$

$$m^2 = \frac{N^2}{(\omega - kU)^2}k^2 + \frac{U''}{(\omega - kU)}k - k^2 - \frac{1}{4H^2}, \tag{2}$$

where U is the basic-state horizontal wind and H is the basic-state scale height. Equations (1) and (2) are the familiar Taylor-Goldstein equation. When the background is sufficiently slowly varying and $m^2 > 0$, m may be interpreted as the vertical wave number. The quantity in parenthesis is the intrinsic frequency. We have made the customary assumption and dropped a term that involves U'. The Brunt-Väisälä frequency is given by

$$N^2 = g\frac{d\log\overline{\theta}}{dz} = \frac{g}{T}\left(\frac{d\overline{T}}{dz} + \frac{g}{C_p}\right), \tag{3}$$

where $\theta = T(p_0/p)^{\kappa}$ is potential temperature, T is temperature, p is pressure, p_0 is a reference value (usually 1000 hPa), and g is gravity. The quantity $\kappa = R/C_p$, where R is the gas constant for air and C_p is the specific heat at constant pressure. For a basic state where U is constant and the atmosphere is isothermal, m is a constant. It is the vertical wave number if $m^2 > 0$ and an inverse attenuation scale if $m^2 < 0$.

[9] As mentioned, we adopt a three-layer model with constant m (i.e., N^2 and U constant) in each layer (whence $U'' = 0$ in (2) and m is constant). For the middle layer, $m^2 > 0$, and for the two surrounding layers, $m^2 < 0$. For convenience, we set $z = 0$ at the center of the inversion. In the middle layer (which we denote as layer 2) the solution of equation (1) has the form

$$\hat{w}_2 = A_2\exp(im_2z) + B_2\exp(im_2z), \tag{4}$$

and in layers 1 and 3 it has the form

$$\hat{w}_i = A_i\exp(\pm\tilde{m}_iz) \quad (i = 1, 3), \tag{5}$$

where $\tilde{m}i^2 = -m_i^2$, the plus sign applies in layer 1, and the minus sign applies in layer 3. The forms of the solutions in layers 1 and 3 implement finiteness of vertically integrated kinetic energy density.

[10] We require that the wave satisfy continuity conditions at the interfaces between the middle layer and the two surrounding layers. These conditions are continuity of w (kinematic condition) and $\hat{p}$ (dynamic condition). The latter implies continuity of $(c - U)w$. The characteristic equation obtained from equations (4) and (5) subject to the continuity conditions is

$$\tan(m_2D) = \frac{\mu_2(\tilde{\mu}_1 + \tilde{\mu}_3)}{\mu_2^2 - \tilde{\mu}_1\tilde{\mu}_3}, \tag{6}$$

where $\mu_2 = (c - U_2)m_2$, $\tilde{\mu}_i = (c - U_i)\tilde{m}_i$ and D is the thickness of the middle region. This must be solved numerically for the eigenvalues ω with the use of equation (2). The eigenfunction satisfying boundary and continuity conditions has the form

$$\hat{w}_2 = A\left(\cos[m_2(z + D/2)] + \frac{\tilde{\mu}_1}{\mu_2}\sin[(m_2(z + D/2))]\right) \tag{7}$$

in layer 2 and

$$\hat{w}_i = A\exp[(-\tilde{m}_i(z \pm D/2))] \tag{8}$$

in layers 1 (minus sign) and 3 (plus sign). The coefficient A is arbitrary. We examine the eigensolutions for choices of N^2 and U (see Table 1).

[11] Whereas the full-wave solutions may include solutions for nonideal ducts that include some leakage of wave energy from the duct, the three-layer model solutions include only fully ducted waves. To force the three-layer model to give eigensolutions where the full-wave model would give partially ducted waves, we reduce the values of N^2 in layers 1 and 3 when necessary; otherwise model parameters are idealizations of the full-wave basic state where observed winds and temperatures

Table 1. Basic-State Parameters for the Three-Layer Model for the Lower Thermospheric Duct and Upper Mesospheric Inversion

Cases	$2\pi/N_1$ (min)	$2\pi/N_2$ (min)	$2\pi/N_3$ (min)	U_1 (m s^1)	U_2 (m s^{-1})	U_3 (m s^{-1})	D^a (km)
Inversion	13.5	4.0	13.5	−20	20	10	6
Lower thermosphere	12.5	4.7	12.5	20	−5	−30	40

[a]Duct thickness.

are used in conjunction with climatological wind and temperature models to prescribe the basic state (see section 2.2). The eigenvalues and the structure in layer 2 are not sensitive to values of N^2 in layers 1 and 3.

2.2. Full-Wave Model

[12] Here we describe the full-wave model and the background states used for various runs.

2.2.1. Model Description

[13] The full-wave model is a linear, steady state model describing the propagation of acoustic-gravity waves upward through a nonisothermal, viscous atmosphere with height-dependent mean winds. The model solves the set of coupled, second-order differential (Navier-Stokes) equations subject to boundary conditions. Given the wave frequency and horizontal wave number the model provides the complex wave perturbations of velocity, pressure and temperature as a function of altitude. The model has been previously used to study gravity wave ducting in the mesosphere/lower thermosphere region and the association with airglow fluctuations [*Walterscheid et al.*, 1999; *Hecht et al.*, 2001; *Hickey*, 2001].

[14] In order that the results in the upper mesosphere not unrealistically reflect the build up of wave amplitude between the ground and the region of low static stability forming the base of the upper mesospheric inversion we implemented a lower sponge layer. This was done by extending the domain to $z = -300$ km and implementing a Rayleigh sponge layer between $z = 0$ and $z = -300$ km. The upper boundary is placed high in the thermosphere (300 km) where viscosity prevents strong reflection from the upper boundary.

2.2.2. Basic States

[15] The background states are defined by combining the predictions of empirical models of temperature and winds [*Hedin*, 1991; *Hedin et al.*, 1996] with data published by *Smith et al.* [2003]. Figure 1 shows the temperature and Brunt-Väisälä frequency squared profile based on the Mass Spectrometer Incoherent Scatter (MSIS) model [*Hedin*, 1991] for the solar and geophysical conditions prevailing at the time of the event (daily $F10.7 = 88$, 81-day average = 120, $Ap = 38$). The profile is lacking a stable layer (inversion) in the upper mesosphere. Note, however, that there is a stable layer in the lower thermosphere with a N^2 peak located near 105 km. This feature is always present in the lower thermosphere and can by itself support ducting [*Walterscheid et al.*, 1999].

[16] The MSIS profile is modified so that below ~50 km the atmosphere is isothermal. This is done (along with modifications in the lower boundary condition described earlier) to avoid ducting at altitudes below the INV. We do not want indications of amplification in the INV and LTD to reflect amplification below. This may be interesting, but is beyond the scope of this study. The resultant profile is shown as the dashed curve in Figure 1a. The first modification to this model is the inclusion of an upper mesospheric inversion. This inversion is an idealized version of the one reported by *Smith et al.* [2003]. This is shown as the solid curve in Figure 1a.

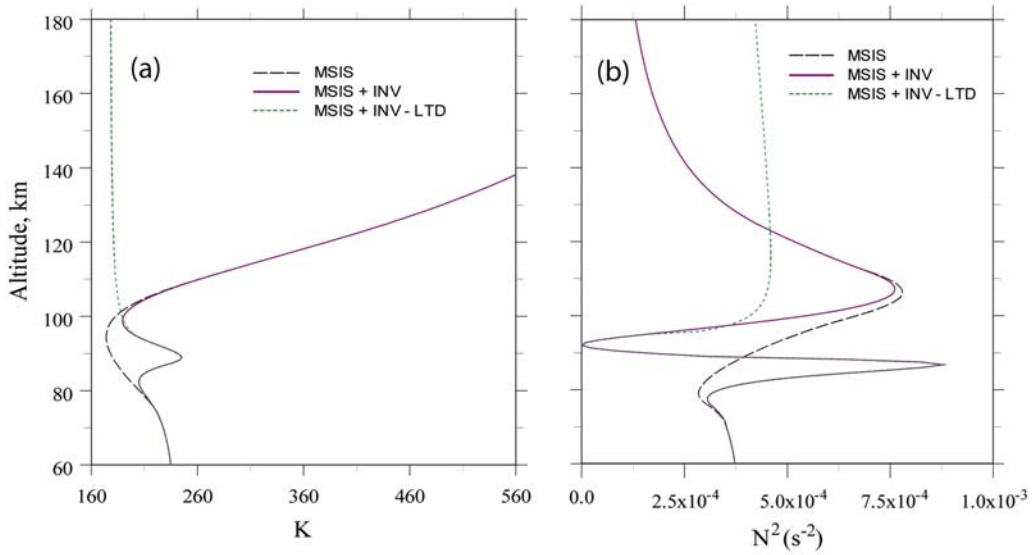

Figure 1. (a) Temperature versus altitude and (b) Brunt-Väisälä frequency squared versus altitude for profiles based on the Mass Spectrometer Incoherent Scatter (MSIS) model [*Hedin*, 1991] for the solar and geophysical conditions prevailing at the time of *Smith et al.*'s [2003] event (dashed curve), for a profile that includes the upper mesospheric inversion (INV) based on the work of *Smith et al.* [2003] (solid curve), and for a profile that includes the INV but excludes the lower thermospheric duct (dotted curve).

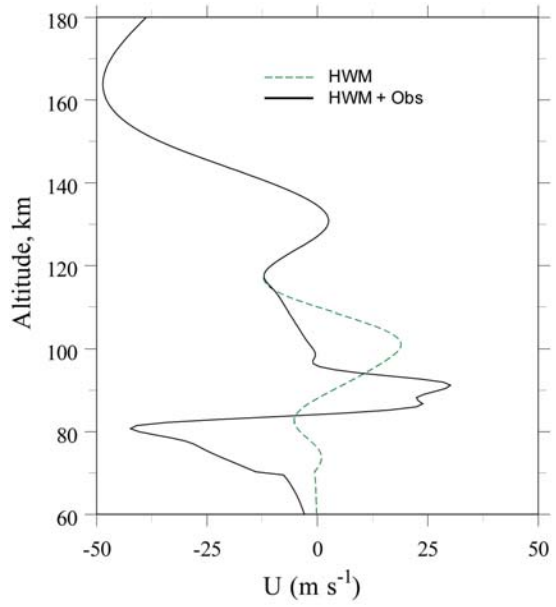

Figure 2. Winds versus height for the altitude region around the two thermal ducts for a profile based on the HWM model (dashed curve) and a profile modified by observations of *Smith et al.* [2003] (solid curve).

[17] It is also interesting to consider what the INV would give if it alone existed as a potential duct. For that purpose we use the following device. Equation (3) may be rewritten as

$$\frac{dT}{dz} - \frac{N^2}{g}T + \frac{g}{Cp} = 0. \tag{9}$$

The solution to equation (9) for N^2 constant is

$$T = \frac{g/Cp}{N_0^2/g} + \left[T_0 - \frac{g/Cp}{N_0^2/g}\right] \exp\left[\frac{N_0^2}{g}(z - z_0)\right], \tag{10}$$

where the subscript "0" refers to the level above which we would like N^2 to be constant.

[18] Equation (10) implies that T increases approximately linearly at first, which is fairly realistic, but grows faster than linear as $z - z_0 \sim N_0^2/g$, which is not realistic. That means that at some point we have to force temperature to be isothermal in order to contain the growth of T. Some distance above the level "0," we modify equation (10) as

$$T = \frac{g/Cp}{N_1^2/g} + \left[T_1 - \frac{g/Cp}{N_1^2/g}\right] \exp\left[\frac{(N_1^2/g)(z - z_1)}{1 + (z - z_1)/\delta Z}\right], \tag{11}$$

which in the large z limit tends to the isothermal value

$$T_\infty = \frac{g/Cp}{N_1^2/g} + \left[T_1 - \frac{g/Cp}{N_1^2/g}\right] \exp\left[\delta Z N_1^2/g\right]. \tag{12}$$

We take z_1 = 95 km and δZ = 5 km.

[19] With equations (10) and (11) we construct a profile with constant $N^2 = N_0^2$ between z_0 and z_1; and decreasing N^2 above z_1 to a constant isothermal value $N^2 = gk/\overline{H}_\infty$. We can eliminate the LTD if we take T_1 to be near the minimum in N^2 between the INV and LTD ducts. The temperature profile with the LTD removed is shown in Figure 1a as the dotted curve.

[20] Figure 1b shows the N^2 profiles corresponding to the temperature profiles shown in Figure 1a: MSIS (dashed curve), MSIS modified by observations (solid curve), and the profile that includes the INV but excludes the lower thermospheric duct (dotted curve). The INV gives an N^2 peak near 87 km and a minimum near 92 km where N^2 is close to zero. The LTD is the feature with an N^2 peak near 105 km seen in the MSIS and modified MSIS profiles.

[21] The winds for the altitude region surrounding the two thermal ducts are given in Figure 2. They are the projection of the horizontal wind model (HWM) winds in the direction of wave propagation for *Smith et al.*'s [2003] event (southward) and the HWM winds modified by a smoothed version of the winds given by *Smith et al.* [2003]. The former is the dashed curve in Figure 2, and the latter is the solid curve. The HWM profile does not show any of the wavelike structure seen in the observed winds between ~60 and 120 km. As for temperature, we modified the profiles in the lower atmosphere to avoid amplitude build up in the stratosphere that would extend into the region of interest. We required the winds to be close to zero below ~50 km.

[22] We examine ducting for five basic states. The simplest basic state is one in which only thermal stratification contributes to ducting (zero winds) and for which the only duct is the one in the lower thermosphere (LTD). This duct is always present and reflects the fact that an increase in temperature that is slower than exponential will give a peak in the N^2 profile. The temperature structure except as noted below is based on the MSIS model [*Hedin*, 1991]. The time and location were chosen to be centered in time and location with respect to the event reported by *Smith et al.* [2003].

[23] The next change in the basic state was to include winds. The first change related to winds was to add climatological winds from the HWM model. This gives winds that are suitable to address the effects of winds on ducting in a general way. They do not fully reflect the vertical variations in the ducting region, but they are probably a good first-order idealization. The HWM winds used in our study were chosen to refer to the same time and place as the MSIS temperatures.

[24] The next revision was to add realism based on lidar wind observations reported by *Smith et al.* [2003]. This is shown as the solid curve in Figure 2. Note that there is considerable shear in the upper mesosphere. The variations in the winds play a crucial role in ducting waves in the INV.

2.2.3. Model Runs

[25] To investigate ducting in the INV and LTD we define an amplification factor following *Schubert and Walterscheid* [1984]. We reference a measure of wave amplitude in the ducts to the wave amplitude in a base run. The base run differs from the experiment in that the base run does not include one or more ducting features that the experiment includes. They also differ in regard to where the waves are forced. In one series of runs the waves are forced in the lower atmosphere and the base run is isothermal. Other runs are forced in the ducts and referenced to runs where one or the other of the ducts is absent, but otherwise similar to the profiles containing both ducts.

Table 2. Matrix of Runs[a]

Case	Duct(s)	Winds	Forcing Level	Levels for KE Ratios (Numerator)	Denominator for KE Ratios	
					Reference Cases	Levels
L/20	LTD	nil	20 km	INV, LTD	T_0/20	50 km
I/20	INV	nil	20 km	INV, LTD	T_0/20	50 km
LI/20	INV, LTD	nil	20 km	INV, LTD	T_0/20	50 km
LH[H$^-$]/20	LTD	±HWM	20 km	INV, LTD	T_0/20	50 km
IH[H$^-$]/20	INV	±HWM	20 km	INV, LTD	T_0/20	50 km
LIH[H$^-$]/20	INV, LTD	±HWM	20 km	INV, LTD	T_0/20	50 km
LIO/20	INV, LTD	HWM/OBS	20 km	INV, LTD	T_0/20	50 km
LIO/I	INV, LTD	HWM/OBS	INV	INV	LO/I	INV
LIO/L	INV, LTD,	HWM/OBS	LTD	LTD	IO/L	LTD
LIO/Z	INV, LTD	HWM/OBS	INV	...	...	...

[a]See text for details on the naming and format convention. Ellipses indicate no reference run (no amplification ratio). KE, kinetic energy.

[26] The amplification factor is defined as

$$A = \frac{[\overline{\rho}\mathbf{u}^2]_{\mathrm{Exp}}}{[\overline{\rho}\mathbf{u}^2]_{\mathrm{Ref}}}, \tag{13}$$

where the subscript "Exp" refers to the experiment (test run), the subscript "Ref" refers to the base run, and $\mathbf{u}^2 = \mathbf{u} \cdot \mathbf{u}$. The ratio A is the ratio of the kinetic energy density (KE) for a test run to that of a reference run evaluated at the same level. The base case for one series of runs is for a windless isothermal background state where energy density is constant. Values of $A > 1$ then indicate amplification due to the vertical variations of winds and temperature. Other base cases are absent a ducting feature contained in the experiment, but are otherwise the same. For example, the experiment may contain both the INV and LTD, while the base case contains only the LTD.

[27] The numerator is the maximum value of KE density in a layer 10 km thick centered on the LTD or INV. This is because the amplitude structure can be quite complicated when wave trapping is strong and we are most interested in amplitude maxima. Since no distinct amplitude maxima occur for the isothermal base case, the denominator for this case is the average value in an 8-km-thick interval centered on the forcing level (20 km). For other base cases, the denominator is calculated the same way as the numerator.

[28] To denote these runs we adopt the format T_1T_2W/F, where T refers to the thermal structure (T_1 = L denotes the LTD, T_2 = I denotes the INV), W refers to the wind profile (W = H denotes the HWM profile, and W = O denotes the HWM profile modified by *Smith et al.*'s [2003] observations), and F refers to the forcing level (F = 20 denotes forcing at 20 km, F = L denotes forcing in the LTD, and F = I denotes forcing in the INV). The special case where there is no reference run (thus no amplification factor) is denoted F = Z. If a duct is missing or if the winds are nil, then the corresponding symbol is omitted. In addition, we perform runs where the HWM winds are reversed to examine Doppler effects further. This case is denoted as H$^-$. The special case of the isothermal basic state is denoted T_0. The specific forcing level for F = I is 86.6 km, and that for F = L is 105 km. These are altitudes near the centers of the respective ducts.

[29] Table 2 is a matrix of the various runs performed. Table 3 is a matrix of the reference runs.

Table 3. Matrix of Reference Runs[a]

Case	Duct(s)	Winds	Forcing Level	Output Levels for KE Ratios
T_0/20	nil	nil	20 km	50 km
LO/I	LTD	HWM/OBS	INV	INV
IO/L	INV	HWM/OBS	LTD	LTD

[a]See text for details on the naming and format conventions.

3. Results

[30] Here we present the results for the idealized three-layer model and the full-wave model run described in section 2.

3.1. Three-Layer Model

[31] Tables 4 and 5 show the solutions for values of wavelength that correspond to observed values during strong ducting events [e.g., *Smith et al.*, 2003, 2005]. Table 4 is for conditions representative of the upper mesospheric inversion, and Table 5 is for conditions representative of the lower thermospheric duct. Values of frequency and phase speed (extrinsic and intrinsic) are shown for the three lowest modes (m = 1, m = 2 and m = 3, respectively). Also shown are the ratios of the vertical wavelength for layer 2 (middle layer) to the layer thickness D (6 km for the upper mesospheric inversion and 25 km for the lower thermospheric duct).

[32] Phase speeds are a strong function of horizontal wavelength, with the faster wave associated with longer wavelengths. Because the eigenfrequency decreases with increasing wavelength, this dependency is not as strong as the dependency expected for longer wavelengths at the same frequency (i.e., the phase speed for the 40-km waves

Table 4. Eigenfrequencies and Phase Speeds for an Idealized Three-Layer Upper Mesospheric Inversion for Various Horizontal Wavelengths and Vertical Modes[a]

$2\pi/k$ (km)	Mode	$2\pi/\omega$ (min)	c (m s^{-1})	L_z/D
20	1	4.2	70.8	3.34
20	2	6.2	53.4	1.45
20	3	8.1	41.4	0.88
30	1	5.2	96.6	3.95
30	2	8.6	58.3	1.60
30	3	11.7	42.9	0.92
40	1	6.1	109	4.39
40	2	11.04	60.4	1.66
40	3	15.4	43.3	0.94

[a]See Table 1.

Table 5. Eigenfrequencies and Phase Speeds for an Idealized Three-Layer Lower Thermospheric Duct for Various Horizontal Wavelengths and Vertical Modes[a]

$2\pi/k$ (km)	Mode	$2\pi/\omega$ (min)	c (m s^{-1})	L_z/D
20	1	5.2	69.1	2.39
20	2	5.5	65.1	1.18
20	3	6.1	59.6	0.78
30	1	5.2	100.5	2.50
30	2	5.9	89.9	1.23
30	3	6.9	77.5	0.81
40	1	5.4	129	2.61
40	2	6.4	110	1.28
40	3	7.9	89.8	0.83

[a]See Table 1.

is not double the phase speed for the 20-km waves).

[33] The phase speeds are ordered by mode, with higher modes having slower speeds for a given k and duct. The ordering reflects the vertical scale with slower waves associated with shorter scales. Comparing ducts this tendency is balanced somewhat by the higher values of N in the upper mesospheric inversion, giving similar phase speeds for the m = 1 mode for the same horizontal phase speed. Otherwise waves in the lower thermospheric duct are faster.

[34] Note that the vertical wavelength in the duct can be ~4 times the duct thickness for the m = 1 mode. This is larger than what is often assumed, by analogy with layers bounded by reflecting surfaces, namely that the fundamental should fit in the duct in the sense that it contains one half wavelength (i.e., $L_z \sim 2D$). However, for reflecting layers there are more degrees of freedom and fitting means satisfying continuity conditions.

[35] The calculated values of phase speed for the m = 3 mode for the upper mesospheric inversion agree reasonably well with the phase speeds reported by *Smith et al.* [2003, 2005], indicating that the observed mode is a higher-order mode and not the fundamental (m = 1, say). On the whole the predicted phase speeds are within the range of reported phase speeds [*Taylor et al.*, 1995b; *Swenson et al.*, 1999; *Nakamura et al.*, 1999; *Smith et al.*, 2000.]

[36] Figure 3 shows the vertical structure of the three lowest modes for a given horizontal wavelength for the upper mesospheric inversion. The vertical structure is plotted as a function of distance from the center of the duct. The lowest mode peaks near the center of the duct, is nearly symmetric about the center and damps toward small values in the surrounding layers. There are no nodes. The m = 2 mode is nearly antisymmetric about the center of the duct where the only node occurs. The m = 3 mode is nearly symmetric has two nodes, both located in the duct about the same distance from the center. The vertical structures of the various modes are similar for other wavelengths and for the lower thermospheric duct.

3.2. Full-Wave Model

[37] The amplification factor was evaluated first for a range of horizontal wavelengths that include the ranges of phase speeds and horizontal wavelengths based on the observations of *Smith et al.* [2003, 2005]. These authors showed that the observed phase speeds are in the approximate range 20–40 m s^{-1} and horizontal wavelengths in the range 20–40 km. We broadened this to include faster larger-scale waves; the total range is 40–100 m s^{-1} in phase speed and 20–60 km in wavelength.

3.2.1. Waves Forced From Below (Isothermal Reference Case)

[38] The waves considered here must propagate (tunnel) through a region of evanescence before they may become resonantly amplified. This can affect the relative amplitudes of various modes in the duct. Those that experience the strongest attenuation will, other factors being about equal, have smaller amplitudes. This affects mainly the lowest mode. However, freer access to the ducts also means weaker trapping in the duct and so waves that can get into the duct with minimal attenuation are weakly ducted and will have reduced amplitudes. This affects mainly the higher modes.

[39] The amplification factor (equation (13)) for the INV for the windless case with only the LTD (L/20) is shown in Figure 4. The reference run is isothermal. The results apply

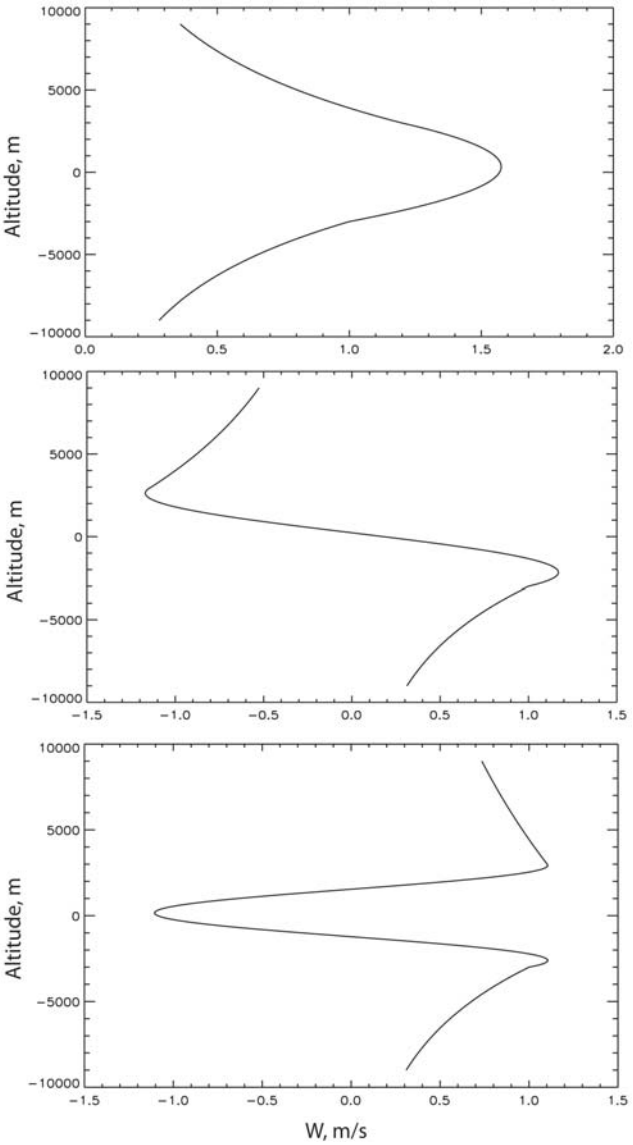

Figure 3. Vertical velocity versus distance from the center of the duct for the three lowest modes of the INV for a horizontal wavelength of 30 km based on the three-layer model.

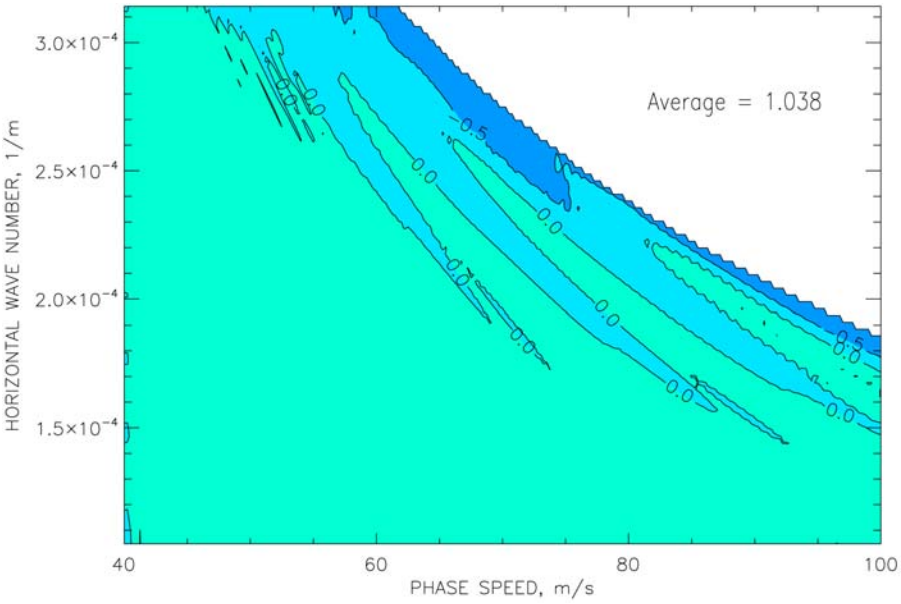

Figure 4. Contour plot of the fractional variation relative to the mean of the amplification factor A given by equation (13) versus phase speed c and horizontal wave number k for INV altitudes for the windless run with only the LTD present (unmodified MSIS) and for an isothermal reference run (case L/20). The numerator of A is the maximum value in a 10-km height interval centered on the N^2 maximum. For reference, wavelengths of 20, 30, 40, and 60 km correspond to values of k of 3.14, 2.09, 1.57, and 1.05 $(10^4 \text{ m})^{-1}$, respectively.

to the LTD. The amplification factor is meaningless when the wave is evanescent at the altitude where the wave is forced (20 km) and for the combinations of c, k where this happens we do not plot results. This gives the white area in the upper right. Figure 4 shows the amplification factor as a fraction of the mean value averaged over the c, k domain plotted. Contour intervals are 0.5. The mean is given in the white area. There is a region of weak amplification that intersects 100 m s^{-1} near a horizontal wavelength of 40 km, and extends up and to the left to near 83 and 25 km where the increase over the mean is zero. Peak values indicate ~50% amplification with respect to the mean. The phase speeds agree fairly well with the results for the idealized model (Table 4) for the $m = 1$ mode. There are other bands of amplification but these are too weak to indicate significant ducting. The average value is close to 1 and indicates that on average the waves in the LTD are not significantly amplified with only the LTD thermal duct present.

[40] Figure 5a shows results for the INV for a profile with both the INV and LTD present (case LI/20). There is little indication of significant ducting, except perhaps for a possible region of ducting that is cut off by the line dividing waves that are evanescent at the source from those that are propagating. We will come back to this later. Figure 5b shows the same case, but for the LTD. Here there is significantly stronger ducting than shown in Figure 4. With respect to the case of the LTD alone, the regions of amplification (including those where amplification was minimal) have been shifted somewhat to the right and are considerably strengthened. The $m = 1$ mode now appears on the boundary of evanescence. The $m = 2$ mode is clearly evident, as well as a third mode and a suggestion of a fourth. The $m = 1$–3 modes are in good to fair agreement with the three-level model.

[41] Note that the average amplification factor in Figure 5b is much reduced from the case with the LTD only. The reason for this is the region of strong evanescence that the INV introduces. This is caused by the region of near-neutral stability above the inversion. A layer of reduced N^2 is a common feature of inversions. Trapping and ducting in the LTD is a strong function of the existence or nonexistence of an inversion in the upper mesosphere.

[42] Figure 6 shows the results for the LTD when we add winds based on the HWM (run LIH/20). The HWM winds have increased the strength of ducting relative to the mean and have allowed a large sequence of modes to exist (up to $m = 7$). This is because of increased values of the refractive index within the LTD due to Doppler effects for the same value of N^2. Thus more modes can fit in the duct without having wave frequencies so low that they cannot be trapped. Note that the average value of A is increased owing to the winds. This is because the winds counteract the effects of the steep lapse rate above the inversion to some extent. This means that not only is ducting greater in relative terms, but it is greater yet in absolute terms. There is no significant effect for the INV (not shown).

[43] When the HWM winds are reversed (run LIH^-/20), or alternatively the direction of wave propagation is reversed, no significant ducting occurs in either layer (not shown). The average value of A is reduced below the zero wind case. With winds that Doppler shift the waves to greater frequency it is more difficult to fit waves in the LTD

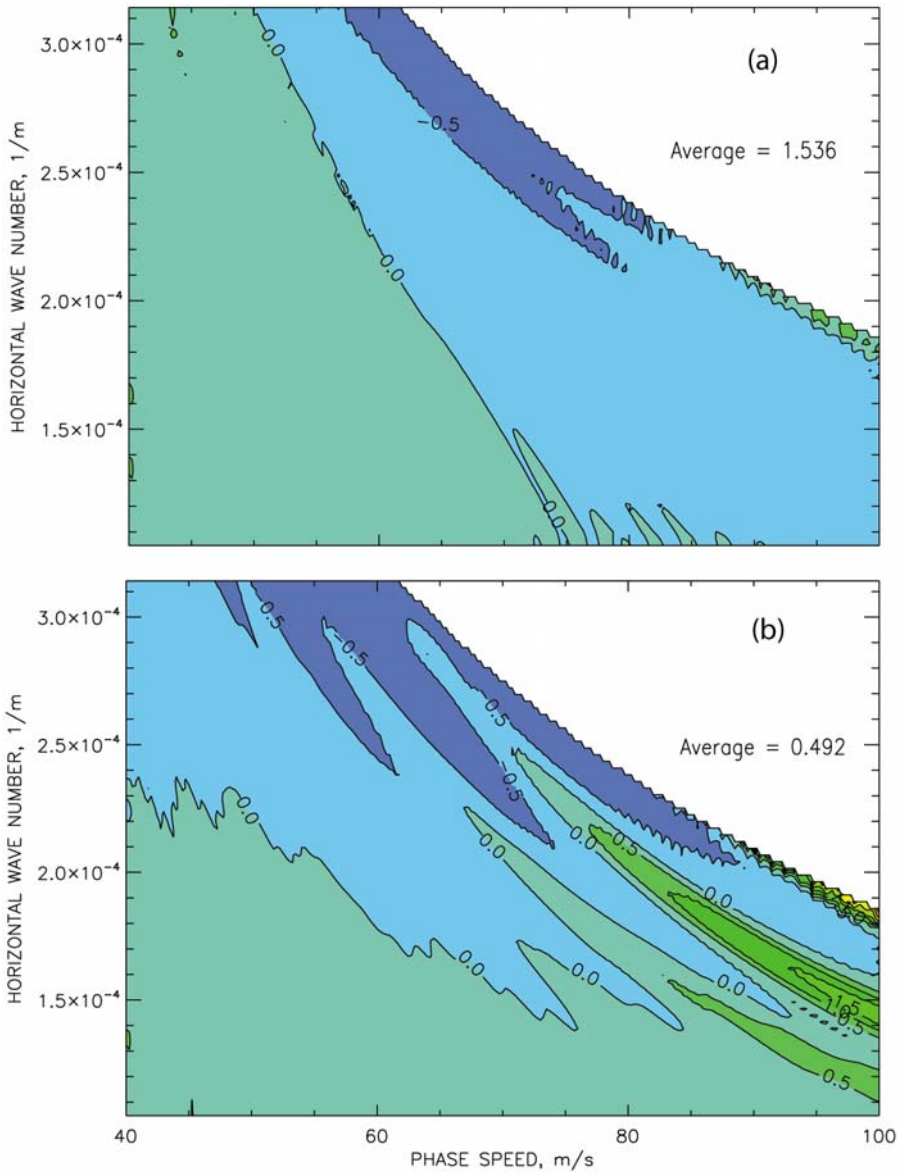

Figure 5. Same as Figure 4 except for (a) INV altitudes and (b) LTD altitudes for both the INV and LTD present (case LI/20). For reference, wavelengths of 20, 30, 40, and 60 km correspond to values of k of 3.14, 2.09, 1.57, and 1.05 $(10^4\ \mathrm{m})^{-1}$, respectively.

or INV or to penetrate regions of stronger evanescence in the c, k region of interest.

[44] Figure 7 shows results in the INV when both thermal ducts are present and when the HWM winds are modified by observed winds (run LIO/20). The effects of the observed winds are dramatic. For the first time strong ducting is apparent for the lower modes (m = 2 and m = 3) and for the first time we see strong ducting (m = 3) that is consistent with *Smith et al.*'s [2003, 2005] observations. Note also that *Smith et al.* [2005] observed that the trailing slower waves were associated with smaller horizontal wavelengths. Note also that the predicted dependence of phase speed on horizontal wavelength is not strong and would allow a train of ducted waves to approximately keep up with the leading disturbance. Thus, our results show that the observations are consistent with the location and orientation of the locus of peak amplification in phase speed–wave number space and are consistent with linear ducted waves.

[45] Figure 8 shows the vertical profiles of amplitude (Figure 8a) and phase (Figure 8b) for the vertical velocity for modes m = 2 and m = 3. (We will deal with the m = 1 mode later.) The amplitude is density weighted to take out the exponential growth with altitude due to decreasing background density. The c, k pairs are points on the locus of amplification for the two modes; c, k = (56.3 m s^{-1}, 2.36 × 10^{-4} m^{-1}) for m = 2 and (44.50 m s^{-1}, 2.17 × 10^{-4} m^{-1}) for m = 3. The m = 2 mode shows a node in the center of the INV in agreement with the results of the three-layer model (Figure 3). For the curve denoted m = 3, there is an additional node. The amplitude maxima are located nearer the duct boundaries than for m = 1, consistent with the modal structure shown in Figure 3; however, for an ideal duct the maxima would be displaced farther toward the duct

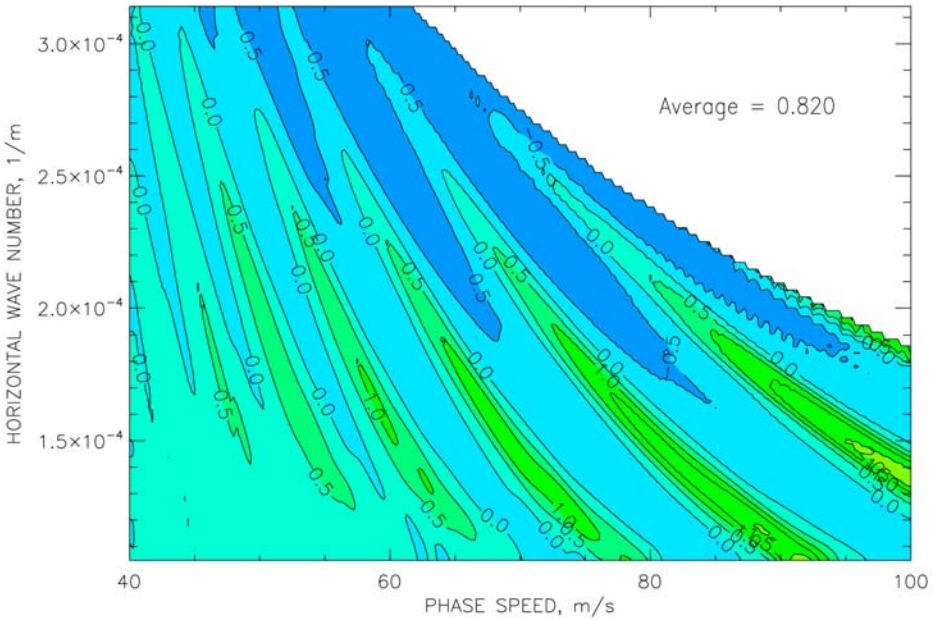

Figure 6. Contour plot of the fractional variation relative to the mean of the amplification factor A given by equation (13) versus phase speed c and horizontal wave number k for LTD altitudes with HWM winds with both the INV and LTD present and an isothermal reference run (case LIH/20). The numerator of A is the maximum value in a 10-km height interval centered on the N^2 maximum. For reference, wavelengths of 20, 30, 40, and 60 km correspond to values of k of 3.14, 2.09, 1.57, and 1.05 $(10^4 \text{ m})^{-1}$, respectively.

boundaries. While the peak amplitudes are strongly confined to the near vicinity of the INV, there is also an indication of weak ducting in the LTD where standing waves show up as a series of minor amplitude maxima and their associated phase rotations.

[46] Figure 9 shows run LIO/20 for the LTD. The results show a sequence of trapped modes similar to those seen in Figure 5b, but the modes $m = 2-4$ are much stronger. There is a clear indication of coupling between the INV and LTD. The upward extension of modes $m = 2$ and 3 seen in Figure 7 are also seen in Figure 9. This leads to the bifurcation of the zones of amplification seen on the right side of Figure 9. A more extreme example of this will be seen later.

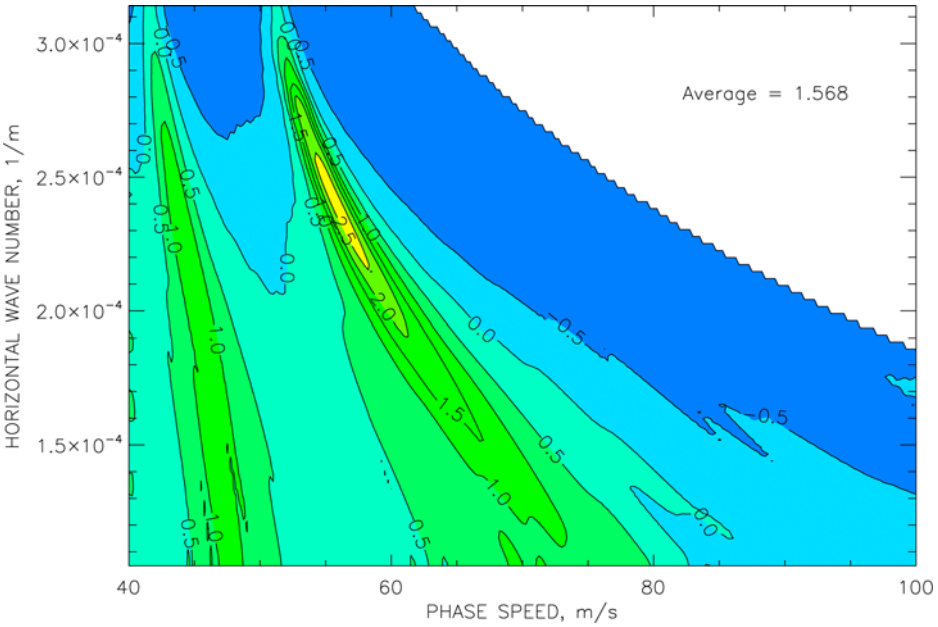

Figure 7. Same as Figure 6 except for INV altitudes when the HWM winds are modified by observed winds (case LIO/20). For reference, wavelengths of 20, 30, 40, and 60 km correspond to values of k of 3.14, 2.09, 1.57, and 1.05 $(10^4 \text{ m})^{-1}$, respectively.

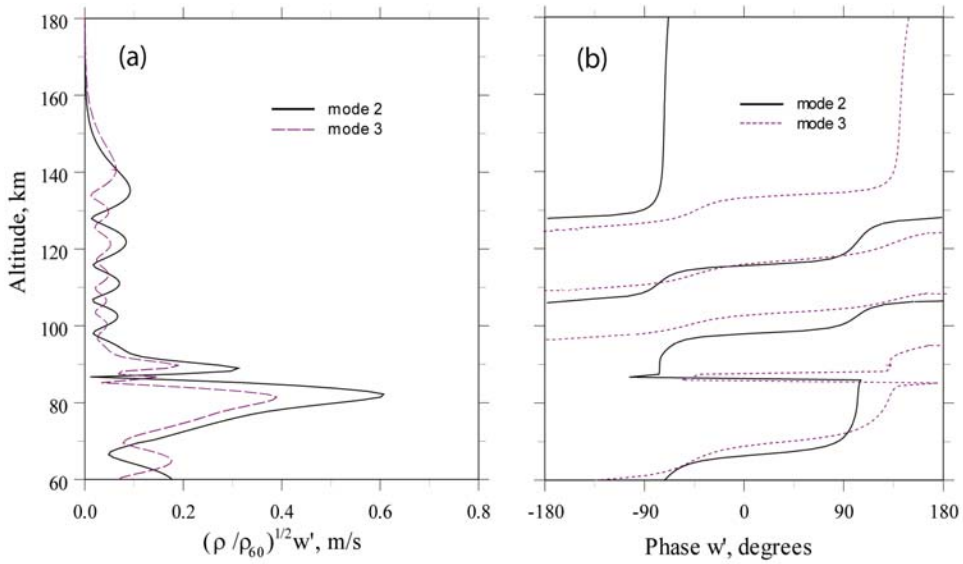

Figure 8. Altitude plots of the (a) vertical velocity amplitude and (b) phase for the $m = 2$ and $m = 3$ modes for the case when the HWM winds are modified by observed winds (the LIO/20 run).

[47] Figure 10 shows the vertical profiles of amplitude and phase of the vertical velocity perturbation w' for $m = 2$, 3 and 4 for the LTD, that is, the first three modes away from the evanescent boundary in the c, k domain shown in Figure 9. The mode denoted $m = 4^*$ is a mode common to the LTD and INV. The four c, k pairs ordered by increasing modal number are (100.00 m s^{-1}, 1.754 $\times$ 10^{-4} m^{-1}), (100.00 m s^{-1}, 1.230 $\times$ 10^{-4} m^{-1}), (81.25 m s^{-1}, 1.257 $\times$ 10^{-4} m^{-1}), and (67.75 m s^{-1}, 1.257 $\times$ 10^{-4} m^{-1}), respectively. The curve denoted $m = 2$ has its largest amplitude in the LTD where the amplitude far exceeds that in the INV, despite attenuation by evanescence between the two layers. In the LTD there is single node within the LTD confirming the $m = 2$ interpretation. Modes $m = 3$, 4 and 4* have 2, 3 and 3 nodes in the LTD, respectively. Modes 3 and 4, like the $m = 2$ mode, are larger in the LTD relative to the INV, but the relative strengths are progressively less the higher the mode. The $m = 4^*$ mode has its largest amplitude in the INV. In the INV we would identify it as $m = 2$ (a single node in the center of the INV).

3.2.2. Waves Forced in Situ

[48] It is also of interest to consider waves forced within the ducts. Here the conditions that favor the higher modes disappear, since it is not necessary to tunnel into the duct.

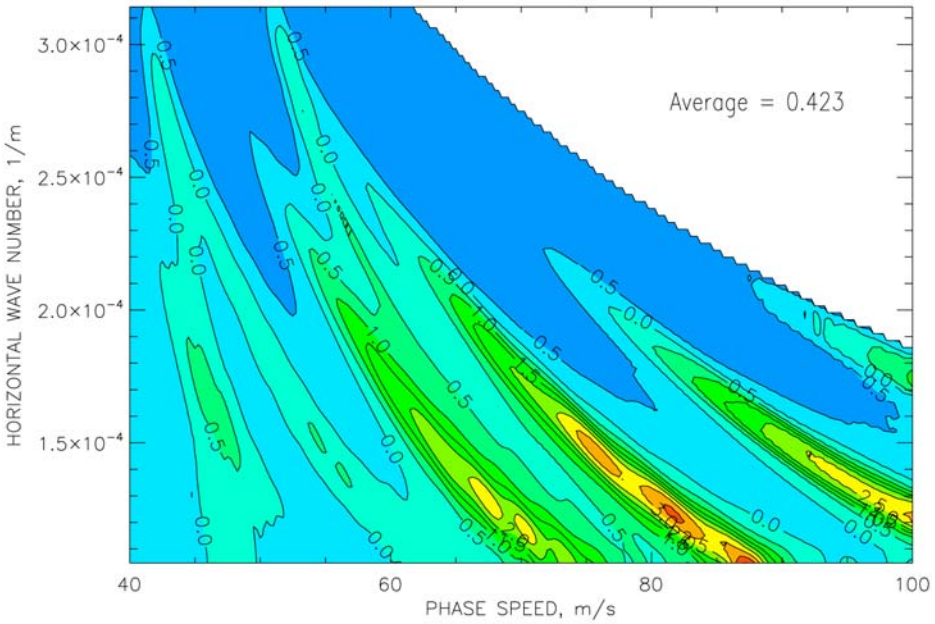

Figure 9. Same as Figure 8 except for LTD altitudes when the HWM winds are modified by observed winds (case LIO/20). For reference, wavelengths of 20, 30, 40, and 60 km correspond to values of k of 3.14, 2.09, 1.57, and 1.05 $(10^4$ m$)^{-1}$, respectively.

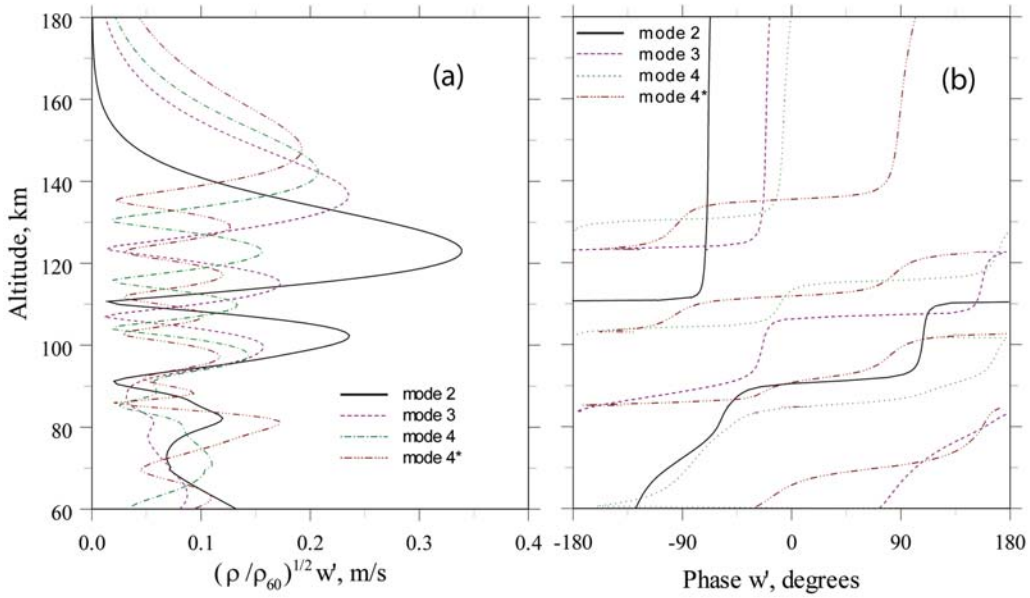

Figure 10. Altitude plots of the (a) vertical velocity amplitude and (b) phase for the $m = 2$, $m = 3$, $m = 4$, and $m = 4^*$ modes for the LIO/20 run (see Figure 9).

For these runs the amplification factor for a wave forced in a certain layer is the run with the thermal duct removed from that layer. For the INV, this is a reference run with only the LTD. For the LTD one must artificially remove the LTD using the means described above.

[49] Figure 11a shows the results for waves forced in the INV ratioed to waves forced in the INV, but with the INV absent (LIO/I). Note that the contour interval is now 2. The ducting is similar to run LIO/20 (Figure 6) for the $m = 2$ and $m = 3$ modes. However, the $m = 1$ mode which is found at the boundary of the plot domain is now very intense. To explore this further we will look at a case in section 3.2.3 without a base run.

[50] Figure 11b shows the results for waves forced in the LTD ratioed to waves forced in the LTD, but with the LTD absent (LIO/L). To remove the LTD the artifact (equation (12)) was used. The ducting is again similar to the run forced from below and referenced to the isothermal run (LIO/20) but the strength of the ducting is ordered differently. Now the ducting is stronger for the lower modes, with the most intense ducting occurring near the boundary denoting evanescence at the forcing for the base case. We will examine the forcing for the $m = 1$ mode without a base case in section 3.2.3.

3.2.3. Waves Forced in Situ With No Base Case

[51] To examine the fundamental ($m = 1$) mode we show runs with KE amplitude rather than KE. Figures 12a and 12b show kinetic energy density ratioed to the mean in the INV and LTD for waves forced in the INV. We dwell on the $m = 1$ mode. None of the waves are evanescent at the source so the entire domain is shown. The contour interval is 1 for the INV and 2 for the LTD. The $m = 1$ mode is very strong at both levels. The results for the INV show no discernible evidence of waves mapped down from the LTD. On the other hand the LTD results show a strong upward extension of the $m = 1$ mode from the INV. The superposition of the $m = 1$ mode native to the LTD and upward extension of the INV $m = 1$ mode cause the bifurcation seen in the in the upper right. The extremely intense feature is where the two modes overlap, suggesting a strong interplay between the two regions. To elucidate this we show the vertical profile of KE for a wave in the center of the region.

[52] Figure 13 shows the vertical profiles of amplitude and phase for w' for the $m = 1$ mode where it coincides with the $m = 1$ INV mode mapped up from below ($c = 82.50$ m s^{-1}, $k = 2.88 \times 10{-}4$ m^{-1}). The absolute values are not meaningful. We see a strong response in both the LTD and INV. There is no phase shift associated with the amplitude minimum between the ducts so it is not a node. No node exists, so that this mode is the $m = 1$ eigenfunction for the combined INV-LTD system.

[53] An obvious question is why, if the $m = 1$ mode is so intense relative to the higher modes, was a higher mode rather than the fundamental observed in the airglow observations reported by *Smith et al.* [2003]. The likely explanation is that the waves in the airglow regions were not forced in situ, but rather were incident from below. An examination of representative refractive index plots for the $m = 1{-}3$ modes (Figure 14) shows that the evanescent barrier below the INV is much stronger for the $m = 1$ mode than for the others. Thus, as discussed above, the appearance of a dominant $m = 1$ mode is favored by in situ forcing. Clearly there are situations when winds, for example, will weaken the evanescent barrier to the extent that the $m = 1$ has fairly easy access to the INV and may in fact be the only mode that can be ducted. Either this or in situ forcing may account for reports of fast waves indicative of the $m = 1$ mode [*Taylor et al.*, 1995b; *Swenson et al.*, 1999; *Nakamura et al.*, 1999; *Smith et al.*, 2000].

3.2.4. Energy Flux Velocity

[54] Here we briefly address the energy flow velocity $U = F/E$, where F is the wave energy flux and E is the wave energy. For freely propagating waves U is the group velocity. The quantity U does not necessarily have the same

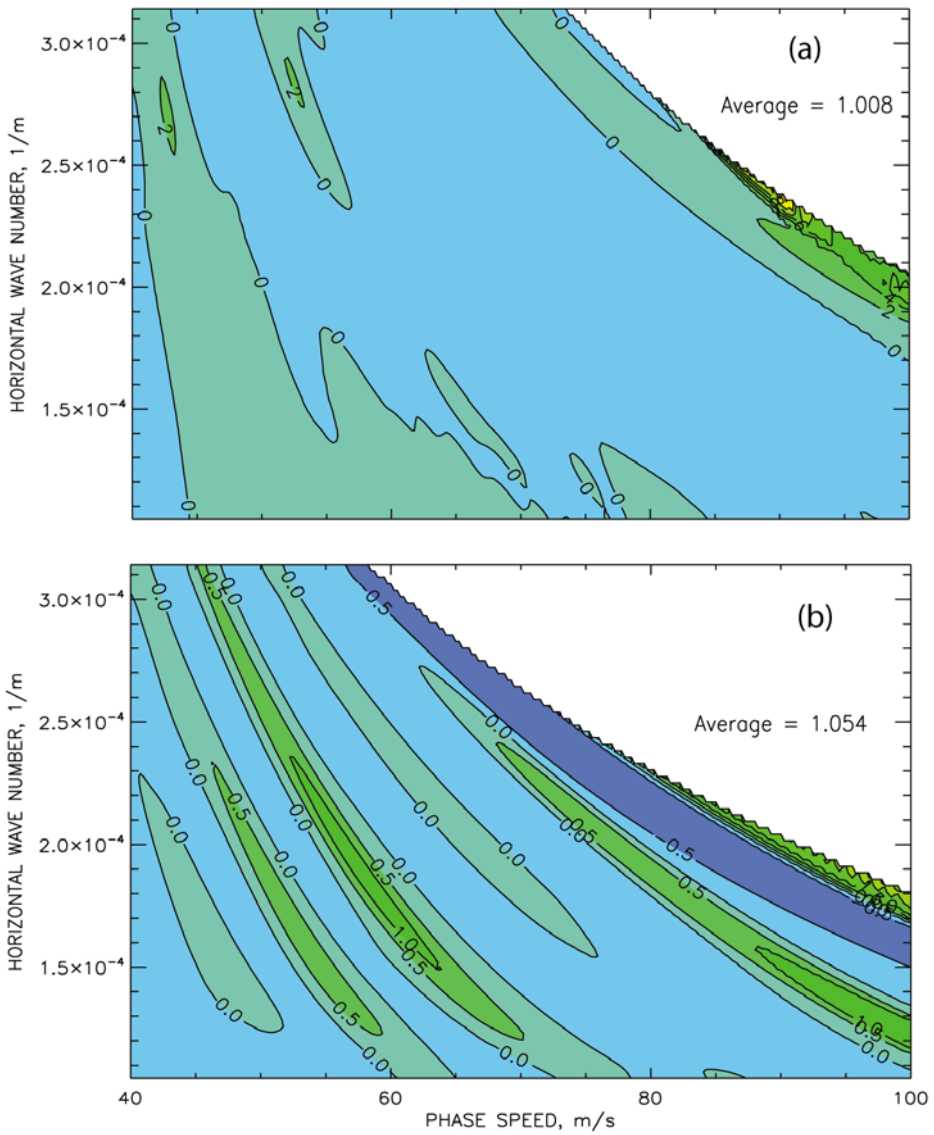

Figure 11. Contour plot of the fractional variation relative to the mean of the amplification factor A given by equation (13) versus phase speed c and horizontal wave number k. (a) For INV altitudes with the INV and LTD present and with HWM winds modified by observations. The waves are forced in the INV and referenced to a run forced at INV altitudes but without the INV present (case LIO/I). The numerator and denominator of A are the maximum values in a 10 km height interval centered on the N^2 maximum in the test run. (b) For LTD altitudes. The waves are forced in the LTD and referenced to a run forced at LTD altitudes but without the LTD present (LIO/L). For reference, wavelengths of 20, 30, 40, and 60 km correspond to values of k of 3.14, 2.09, 1.57, and 1.05 $(10^4\text{m})^{-1}$, respectively.

ordering in terms of mode that the phase velocity has (lower-order modes having faster velocities). Deducing U from the group velocity from our simulations cannot be done. The solutions contain a mixture of propagating, standing and evanescent waves. Thus we have calculated U by means of a direct calculation of F and E [*Walterscheid and Hecht*, 2003]. We calculate U for two modes where only thermal ducting is involved and for two modes where a mixture of thermal and Doppler ducting is involved. The former is the case with the INV and LTD with no winds (LI/20); the latter case is also with the INV and LTD, but with observed winds (LI0/20). Where background winds are involved we use the generalized wave energy flux that includes the flux induced by the mean flow [*Holton*, 1975; *Yu and Hickey*, 2007]. We perform the calculation for the INV and average U over the layer 86 ± 4 km. By averaging, we reduce the sensitivity of the results to details of the duct.

[55] We examine values of U for a neighboring pair of modes: for each case we examine two (c, k) combinations for a fixed value of k near neighboring peaks in amplification. The (c, k) pair for the thermal duct are (86 m s^{-1}, 1.5×10^{-4} m^{-1}) for the higher mode and (98 m s^{-1}, 1.5×10^{-4} m^{-1}) for the lower mode. This corresponds to a common wavelength of 41.9 km and periods of 8.1 and 7.1 min, respectively. We find U is 49.4 m s^{-1} for the higher

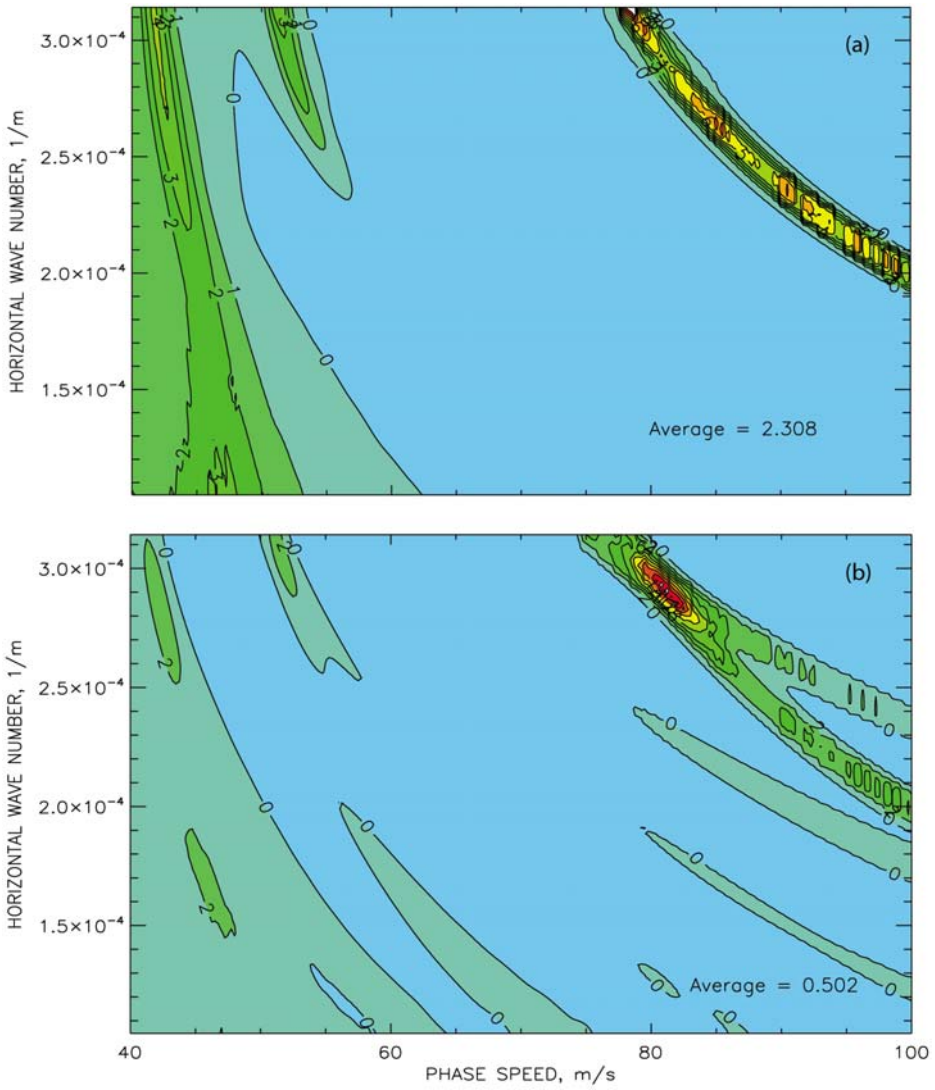

Figure 12. (a) Contour plot of kinetic energy density in the INV ratioed to the mean versus phase speed c and horizontal wave number k for waves forced in the INV (case LIO/Z). (b) Same as Figure 12a except for LTD. For reference, wavelengths of 20, 30, 40, and 60 km correspond to values of k of 3.14, 2.09, 1.57, and 1.05 $(10^4\text{m})^{-1}$, respectively.

mode and 41.6 m s^{-1} for the lower mode. Thus the energy flow velocities are less than the phase velocity and the order is reversed with the higher mode being faster [*Snively and Pasko*, 2008]. This is what one would infer qualitatively from the dispersion relation.

[56] For the duct with observed winds the (c, k) pairs are (44 m s^{-1}, 2.4×10^{-4} m^{-1}) for the higher mode and (56 m s^{-1}, 2.4×10^{-4} m^{-1}) for the lower mode. This corresponds to a common wavelength of 26.2 km and respective periods of 9.9 and 7.8 min. We find U is 30.8 m s^{-1} for the higher mode and 29.0 m s^{-1} for the lower mode. Again the energy flow velocities are less than phase velocity, but the energy flow velocities are similar, with the lower mode being slightly faster. The effect of winds is consistent with the work of *Snively et al.* [2007]. These authors performed time-dependent simulations and found that for instances of pure Doppler ducting the lower-order modes run out ahead of the higher ones. Thus, for the background wind profiles considered Doppler effects accelerate the lower-order modes relative to the higher ones.

[57] The question of group velocity has implications for the ordering of modes in a wave train. If an initial disturbance separates into modes then the ordering should reflect U, with the lower-order modes leading for thermal ducting and the higher-order modes leading when Doppler ducting dominates. The fact that U can be similar for different modes makes the appearance of a wave train, such as observed by *Smith et al.* [2003], explicable in terms of separation into modes. With an appropriate combination of thermal and Doppler effects the appearance of a wave train might be explained by modal separation.

4. Summary and Conclusions

[58] We examine ducting by winds and thermal structure in the upper mesosphere and lower thermosphere. Strong

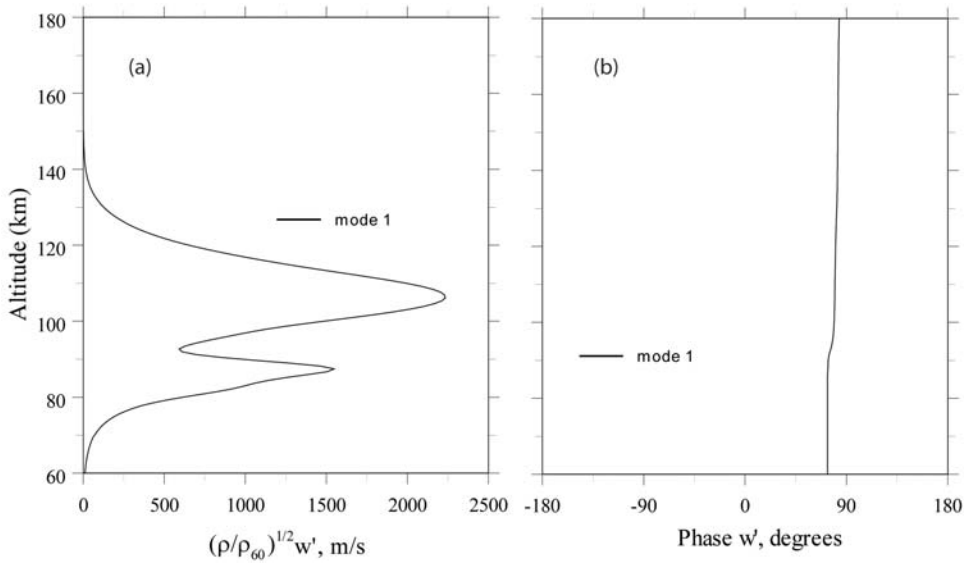

Figure 13. Altitude plots of the (a) vertical velocity amplitude and (b) phase in the region where the m = 1 modes excited in the INV and LTD combine to give an intense amplification in the LTD (see Figure 12b).

ducting events seem to be associated with the existence of an inversion in the upper mesosphere. In addition, there is a peak in the static stability located in the lower thermosphere not too far above the inversion. We denote the former by INV and the latter by LTD.

[59] We have performed a numerical study of ducted waves in these regions using a simple theoretical model and a more general full-wave model. The theoretical model is a three-layer model where the eigenvalues and eigenfunctions can be found as solutions to an analytical expression. The solutions are obtained for idealized basic-state conditions derived from climatological wind and temperature models and observations reported by *Smith et al.* [2003]. The results indicate the existence of a multiplicity of solutions for a given horizontal wavelength, each solution corresponding to waves with a different number of nodes in the vertical variation of the vertical velocity. The fundamental (m = 1) has zero nodes, the first harmonic (m = 2) has 1 node and so forth. Each higher mode is slower than the previous one, and for a given mode larger horizontal wavelengths are associated with faster phase speed, but the relation is not linear, with the dependence being stronger the longer the wavelength. Phase speeds for a horizontal wavelength of 30 km are 97, 58 and 43 m s^{-1} for the m = 1, 2 and 3 modes, respectively, for the INV and 100, 90 and 77 m s^{-1} for the LTD. Predicted phase speeds for the INV m = 3 mode are in reasonable agreement with observations [*Smith et al.*, 2003, 2005].

[60] An interesting feature of the results is the vertical wavelength of the fundamental in the duct (layer 2) compared to the thickness of the duct. It is often assumed that ducted waves are those that approximately fit in the duct in the sense that an integer or half integer number of waves is contained in the duct, with the fundamental having approximately one-half wavelength between duct boundaries. "Fitting" however means that the waves satisfy continuity conditions between layers and this gives the result that the wavelength of the fundamental is $\sim$3–4 times the duct thickness rather than $\sim$2 times.

[61] To characterize the ducted modes with a more general model we use a full-wave model with realistic wind and temperature structure and dissipation and focus on conditions that give ducting INV and LTD. We analyze ducted waves for backgrounds with increasing realism, starting with a climatological temperature profile [*Hedin*, 1991] where the only duct is the one in the lower thermosphere, since this duct is always present. In succession, we add an upper mesospheric inversion based on observations during a strong ducting event [*Smith et al.*, 2003], climatological winds [*Hedin et al.*, 1996], and winds in the upper

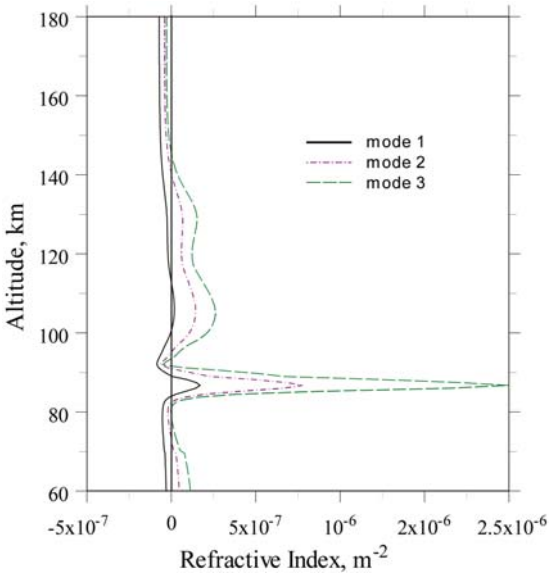

Figure 14. Altitude plots of representative refractive index plots for the m = 1, 2, and 3 modes shown in Figure 12a.

mesosphere based on the observations from *Smith et al.* [2003]. The observations of *Smith et al.* [2003] are similar to a number of other observations in showing a train of waves following a sharp front in airglow intensity and which have been interpreted as manifestations of undular bores [*She et al.*, 2004; *Smith et al.*, 2006; *Taylor et al.*, 1995a; *Dewan and Picard*, 1998, 2001].

[62] We examine ducting for phase speeds between 40 and 100 m s^{-1} and horizontal wavelengths between 20 and 60 km. These ranges include the main part of the observations of which we are aware [*She et al.*, 2004; *Smith et al.*, 2000, 2006; *Taylor et al.*, 1995a, 1995b; *Swenson et al.*, 1999; *Nakamura et al.*, 1999]. We find that without winds only the LTD supports ducting of waves forced from below. However, the ducting is not strong. The inclusion of climatological winds projected in the direction of wave propagation strengthens ducting in the LTD. With HWM winds the LTD supports a large number of modes (up to $m = 7$) in the c, k regions of interest. Ducting is absent when propagation is opposed to the projected winds.

[63] When observed winds and temperatures are included strong ducting is evident in both ducting regions. In our simulations the winds do not create separate ducts; mainly they modify the resonant properties of the thermal ducts. The ducted waves agree well with the three-layer model in terms of phase speed. For waves forced below the INV the strongest ducted modes in the INV are higher modes with slower phase speeds. The phase speeds associated with the INV $m = 3$ mode agree well with the observations of *Smith et al.* [2003, 2005], who reported waves with phase speeds in the range ~40–60 m s^{-1} and horizontal wavelengths in the range ~20–30 km, or somewhat greater (averaging 30 km in one instance). This supports the idea that the observed waves were ducted waves. The observations indicate a tendency for slower waves in the wave train to have shorter wavelengths. At the same time in order for the waves to approximately keep up with the leading disturbance (i.e., be bore-like) the phase speeds cannot be a strong function of wavelength. Our results show this is consistent with the locus of peak amplification for the $m = 3$ INV mode and is consistent with a linear explanation. This does not, however, preclude a nonlinear contribution (possibly dominant) to the behavior observed by *Smith et al.* [2003]. Our results also indicate that it can be very difficult for bore-like behavior to be maintained for lower modes ($m < 3$) and longer wavelengths (>30 km), because there can be a strong dependence of phase speed on horizontal wavelength.

[64] For waves forced in the INV we find an intense and strongly dominant fundamental mode. This mode is fast having phase speeds ~100 m s^{-1} for a horizontal wavelength of 30 km in the INV and is much faster in the LTD. That the fundamental is not seen in *Smith et al.*'s [2003] observations indicates that the waves were forced from below. This is because the fundamental is associated with much stronger attenuation due to evanescence in the layer below the INV than the higher modes. However, *Munasinghe et al.* [1998] examined the wave observed by *Taylor et al.* [1995a] and identified the wave as an $m = 3$ ducted mode that was excited in situ in the LTD.

[65] Our results show that the two ducts can communicate with dramatic results. The upward extensions of waves ducted in the INV are seen in the LTD. This is particularly significant in the case of in situ forcing in the INV. This excites a fundamental in the LTD and combines with the upward extension of the fundamental in the INV. The result is regions in c, k space where amplification is particularly intense. We remark that some instances of strongly ducted waves [e.g., *Smith et al.*, 2003; *Taylor et al.*, 1995a] appear cleaner than would be consistent with a high degree of coupling between ducts. The strongest coupling occurs for in situ forcing and is rather weak for forcing from below. The degree of coupling also depends on the extent to which a significant evanescent barrier exists between the ducts and despite relying on observations we may have underestimated the degree of evanescent attenuation between the ducts when strong ducting events such as these occur.

[66] **Acknowledgments.** This project was supported by NASA grants NAG5-9193 and NNX08AM13G and by NSF grant ATM 0737557.

References

Chimonas, G., and C. O. Hines (1986), Doppler ducting of atmospheric gravity waves, *J. Geophys. Res.*, *91*, 1219–1230, doi:10.1029/JD091iD01p01219.

Dewan, E. M., and R. H. Picard (1998), Mesospheric bores, *J. Geophys. Res.*, *103*, 6295–6305, doi:10.1029/97JD02498.

Dewan, E. M., and R. H. Picard (2001), On the origin of mesospheric bores, *J. Geophys. Res.*, *106*, 2921–2927, doi:10.1029/2000JD900697.

Francis, S. H. (1973), Acoustic-gravity modes and large-scale traveling ionospheric disturbances of a realistic, dissipative atmosphere, *J. Geophys. Res.*, *78*, 2278–2301, doi:10.1029/JA078i013p02278.

Hecht, J. H., S. K. Ramsay Howat, R. L. Walterscheid, and J. R. Isler (1995), Observations of variations in the OH Meinel nightglow during ALOHA 93, *Geophys. Res. Lett.*, *22*, 2817–2820, doi:10.1029/95GL03019.

Hecht, J. H., R. L. Walterscheid, M. P. Hickey, and S. J. Franke (2001), Climatology and modeling of quasi-monochromatic atmospheric gravity waves observed over Urbana, Illinois, *J. Geophys. Res.*, *106*, 5181–5195, doi:10.1029/2000JD900722.

Hedin, A. E. (1991), Extension of the MSIS thermosphere model into the middle and lower atmosphere, *J. Geophys. Res.*, *96*, 1159–1172, doi:10.1029/90JA02125.

Hedin, A. E., et al. (1996), Empirical wind model for the upper, middle and lower atmosphere, *J. Atmos. Terr. Phys.*, *58*, 1421–1447, doi:10.1016/0021-9169(95)00122-0.

Hickey, M. P. (2001), Airglow variations associated with nonideal ducting of gravity waves in the lower thermosphere region, *J. Geophys. Res.*, *106*, 17,907–17,917, doi:10.1029/2001JD900182.

Holton, J. R. (1975), *The Dynamic Meteorology of the Stratosphere and Mesosphere*, *Meteorol. Monogr.*, vol. 15, no. 37, 218 pp., Am. Meteorol. Soc., Boston, Mass.

Isler, J. R., M. J. Taylor, and D. C. Fritts (1997), Observational evidence of wave ducting and evanescence in the mesosphere, *J. Geophys. Res.*, *102*(D22), 26,301–26,313.

Munasinghe, G., H. Hur, T. Y. Huang, A. Bhattachryya, and T. F. Tuan (1998), Application of the dispersion formula to long- and short-period gravity waves: Comparisons with ALOHA-93 data and an analytical model, *J. Geophys. Res.*, *103*(D6), 6467–6481.

Nakamura, T., A. Higashikawa, T. Tsuda, and Y. Matsushita (1999), Seasonal variations of gravity wave structures in OH airglow with a CCD imager at Shigaraki, *Earth Planets Space*, *51*, 897–906.

Richmond, A. D. (1978), The nature of gravity wave ducting in the thermosphere, *J. Geophys. Res.*, *83*, 1385–1389, doi:10.1029/JA083iA04p01385.

Schubert, G., and R. L. Walterscheid (1984), Propagation of small-scale acoustic gravity waves in the Venus atmosphere, *J. Atmos. Sci.*, *41*, 1202–1213, doi:10.1175/1520-0469(1984)041<1202:POSSAG>2.0.CO;2.

She, C. Y., T. Li, B. P. Williams, and T. Yuan (2004), Concurrent OH imager and sodium temperature/wind lidar observation of a mesopause region undular bore event over Fort Collins/Platteville, Colorado, *J. Geophys. Res.*, *109*, D22107, doi:10.1029/2004JD004742.

Smith, S. M., M. Mendillo, J. Baumgardner, and R. R. Clark (2000), Mesospheric gravity wave imaging at a subauroral site: First results from Millstone Hill, *J. Geophys. Res.*, *105*, 27,119–27,130.

Smith, S. M., M. J. Taylor, G. R. Swenson, C.-Y. She, W. Hocking, J. Baumgardner, and M. Mendillo (2003), A multidiagnostic investigation of the mesospheric bore phenomenon, *J. Geophys. Res.*, *108*(A2), 1083, doi:10.1029/2002JA009500.

Smith, S. M., J. Friedman, S. Raizada, C. Tepley, J. Baumgardner, and M. Mendillo (2005), Evidence of mesospheric bore formation from a breaking gravity wave event: Simultaneous imaging and lidar measurements, *J. Atmos. Sol. Terr. Phys.*, *67*, 345–356, doi:10.1016/j.jastp.2004.11.008.

Smith, S. M., J. Sheer, S. Raizada, E. Reisin, J. Baumgardner, and M. Mendillo (2006), Characterization of exceptionally strong mesospheric wave events using all-sky and zenith airglow observations, *J. Geophys. Res.*, *111*, A09309, doi:10.1029/2005JA011197.

Snively, J. B., and V. P. Pasko (2008), Excitation of ducted gravity waves in the lower thermosphere by tropospheric sources, *J. Geophys. Res.*, *113*, A06303, doi:10.1029/2007JA012693.

Snively, J. B., V. P. Pasko, M. J. Taylor, and W. K. Hocking (2007), Doppler ducting of short-period gravity waves by midlatitude tidal wind structure, *J. Geophys. Res.*, *112*, A03304, doi:10.1029/2006JA011895.

Swenson, G. R., J. Qian, J. M. C. Plane, P. J. Espy, M. J. Taylor, D. N. Turnbull, and R. P. Lowe (1998), Dynamical and chemical aspects of the mesospheric Na "wall" event on October 9, 1993 during the airborne lidar and observations of Hawaiian airglow (ALOHA) campaign, *J. Geophys. Res.*, *103*, 6361–6380, doi:10.1029/97JD03379.

Swenson, G. R., R. Haque, W. Yang, and C. S. Gardner (1999), Momentum and energy fluxes of monochromatic gravity waves observed by an OH imager at Starfire Optical Range, New Mexico, *J. Geophys. Res.*, *104*, 6067–6080, doi:10.1029/1998JD200080.

Taylor, M. J., D. N. Turnbull, and R. P. Lowe (1995a), Spectrometric and imaging measurements of a spectacular gravity wave event observed during the ALOHA-93 campaign, *Geophys. Res. Lett.*, *22*, 2849–2852, doi:10.1029/95GL02948.

Taylor, M. J., M. B. Bishop, and V. Taylor (1995b), All-sky measurements of short period gravity waves imaged in the OI (557.7 nm) and near infrared OH and O2(0,1) nightglow emissions during the ALOHA-93 campaign, *Geophys. Res. Lett.*, *22*, 2833–2836, doi:10.1029/95GL02946.

Walterscheid, R. L., and J. H. Hecht (2003), A reexamination of evanescent acoustic-gravity waves: Special properties and aeronomical significance, *J. Geophys. Res.*, *108*(D11), 4340, doi:10.1029/2002JD002421.

Walterscheid, R. L., J. H. Hecht, R. A. Vincent, I. M. Reid, J. Woithe, and M. P. Hickey (1999), Analysis and interpretation of airglow and radar observations of quasi-monochromatic gravity waves in the upper mesosphere and lower thermosphere over Adelaide, Australia (35° S, 138° E), *J. Atmos. Sol. Terr. Phys.*, *61*, 461–478, doi:10.1016/S1364-6826(99)00002-4.

Yu, Y., and M. P. Hickey (2007), Simulated ducting of high-frequency atmospheric gravity waves in the presence of background winds, *Geophys. Res. Lett.*, *34*, L11103, doi:10.1029/2007GL029591.

M. P. Hickey, Department of Physical Sciences, Embry-Riddle Aeronautical University, 600 S. Clyde Morris Boulevard, Daytona Beach, FL 32114, USA.

R. L. Walterscheid, Space Science Applications Laboratory, The Aerospace Corporation, P.O. Box 92957, Los Angeles, CA 90009, USA. (Richard.Walterscheid@aero.org)